Bayesian Network-based Mendelian Randomization for Variant Prioritization and Phenotypic Causal Inference

Supplementary Notes

SN1   Details about BNMR model

In the following we use notations in the calligraphic font $\mathcal{Z}$ to represent the set of variants, the bold font $\boldsymbol{Z}$ to represent the random vector of corresponding variants, and Italic capital letter Z to represent single variant.

As shown in Figure 1 & S1, in the learning stage, we introduce the DIE partitioning of the variant set $\mathcal{Z}$ according to the relationships with the exposure of interest X

$$\mathcal{Z} = \mathcal{Z}_D \cup \mathcal{Z}_I \cup \mathcal{Z}_E. \tag{S.1}$$

For each subject, the genotype of the whole genome is a random vector $\boldsymbol{Z} = (\boldsymbol{Z}_D^T, \boldsymbol{Z}_I^T, \boldsymbol{Z}_E^T)^T$ with each element equal to 0, 1, or 2, where $\boldsymbol{Z}_D$, $\boldsymbol{Z}_I$, and $\boldsymbol{Z}_E$ stand for the random vectors containing variants in subsets $\mathcal{Z}_D$, $\mathcal{Z}_I$, and $\mathcal{Z}_E$. variants in $\mathcal{Z}_D$ directly affect the exposure, variants in $\mathcal{Z}_I$ indirectly affect the exposure through gene interaction or linkage, and variants in $\mathcal{Z}_E$ do not affect the exposure. In other words, $\boldsymbol{Z}_E$ is independent with X ($X \perp\!\!\!\perp \boldsymbol{Z}_E$), $\boldsymbol{Z}_I$ is independent with X given $\boldsymbol{Z}_D$ ($X \perp\!\!\!\perp \boldsymbol{Z}_I | \boldsymbol{Z}_D$).
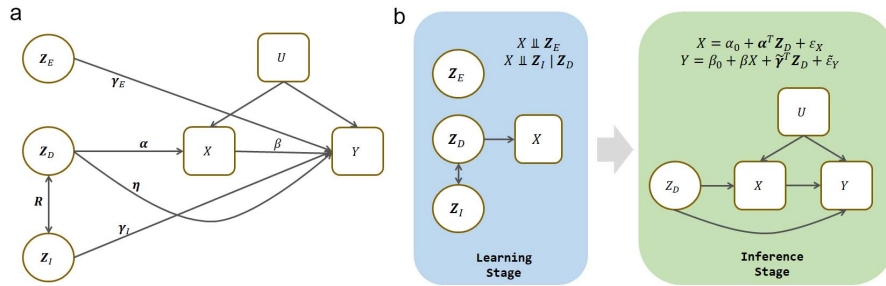

Figure S1: Notations in BNMR model.

The three subsets can be distinguished via a directed acyclic graph (DAG) under the causal Markov, faithfulness, and sufficiency assumptions [1].

- Causal Markov assumption: Any node in a given network is conditionally independent of its non-descendents, given its parents. In other words, all variables that are d-separated in a DAG will be conditionally independent in the corresponding probability distribution.

- Causal Faithfulness assumption: No conditional independence relations other than the ones entailed by the Markov assumption are present in the population distribution. In other words, only the variables that are d-separated in a DAG will be independent.

- Causal Sufficiency assumptions: There are no unmeasured common causes of any pair of variables that are under consideration.

We transform the subset partition problem into a the structure learning of Bayesian networks (BN). A BN is a DAG $\mathcal{G} = \{\mathcal{V}, \mathcal{E}\}$ where nodes represent the variables while edges represent the conditional dependencies, with a collection of conditional probability distributions $\mathcal{O}$ that define the behavior of each variable given its parents. Scored-based approaches determine the optimal network by search all candidate graphs and maximizing the network score, such as the Bayesian information criterion (BIC) and the Bayes Dirichlet equivalent uniform (BDeu). These methods are computationally expensive, although greedy heuristics are often adopted to restricted the number of candidates. Meanwhile, constraint-based approaches employ a series of conditional independence tests to identify the edge constraints between nodes and then determine the directions by additional rules. It is usually faster, but often traps into the dilemma of Markov equivalent classes, on account of the same conditional independent patterns between the confounder and mediator [2]. Various algorithms can be implemented with R package bnlearn [3]

Since variants are causes of traits naturally according to the central dogma of molecular biology, the structure learning process can be further simplified to the determination of graph skeleton. Variants in $\mathcal{Z}_I$ and exposure X are D-separated by variants in $\mathcal{Z}_D$, and only the latter can be parents of X in the causal graph. Therefore, we identify variants in $\mathcal{Z}_D$ by scanning those nodes adjacent to X in the graph. The direction of edge variant-exposure is restricted as $Z_i \rightarrow X$ according to the central dogma of molecular biology. To simplify the computation, we introduce random graph forest (RGF), in which we sample n_s subjects and p_s features each time, and learn the network structure parallelly in all r subsamples. We then calculate the frequency of edge $Z_i - X$ in all subgraphs. The frequency is named as the adjacency score of Z_i, as an relative assessment of the relevance strength. Variants with the largest adjacency scores will be identified as Z_D and selected as IVs in the inference stage.

A quantitative trait is determined by both genotypic and environmental effects: $T = G + E$, where the mean environmental effect is usually taken to be zero. Therefore, when the genotypes are fixed, the trait follows a Gaussian

distribution $T|G \sim \mathcal{N}(G, \sigma_E^2)$. Therefore, X is determined by variants in $\mathcal{Z}_D$ and other environmental factors. Assuming linearity and no interaction, we have,

$$X = \alpha_0 + \boldsymbol{\alpha}^T \boldsymbol{Z}_D + \varepsilon_X, \tag{S.2}$$

where α represents the corresponding effect coefficients for X. Similarly, the outcome Y may be influenced by variants in $\mathcal{Z}_D$, $\mathcal{Z}_I$, and $\mathcal{Z}_E$,

$$Y = \gamma_0 + \boldsymbol{\gamma}_D^T \boldsymbol{Z}_D + \boldsymbol{\gamma}_I^T \boldsymbol{Z}_I + \boldsymbol{\gamma}_E^T \boldsymbol{Z}_E + \varepsilon_Y, \tag{S.3}$$

where β represents the corresponding effect coefficients for Y, and the error terms ε_X and ε_Y are correlated, but independent with $\boldsymbol{Z}$. Due to the horizontal pleiotropy, variants $Z_D \in \mathcal{Z}_D$ can affect Y through two different pathways: the vertical pleiotropy, which means Z_D affects Y through the exposure we studied (X), i.e., the causal pathway between X and Y ($Z_D \xrightarrow{\boldsymbol{\alpha}} X \xrightarrow{\beta} Y$); as well as the horizontal pleiotropy, which means Z_D affects the outcome directly or through other phenotypes ($Z_D \xrightarrow{\boldsymbol{\eta}} Y$). Under the assumption that horizontal pleiotropy effects are independent of the effects via the exposure (the InSIDE assumption) [4], we have,

$$\boldsymbol{\gamma}_D = \beta\boldsymbol{\alpha} + \boldsymbol{\eta}, \tag{S.4}$$

where β stands for the causal effect between exposure X and outcome Y, and $\boldsymbol{\eta}$ stands for the horizontal pleiotropy effects on Y of $\boldsymbol{Z}_D$.

For other variants, since $\boldsymbol{Z}_I$ is correlated to $\boldsymbol{Z}_D$ via gene interaction or linkage, we use $\boldsymbol{Z}_D$ to represent $\boldsymbol{Z}_I$ as

$$\boldsymbol{Z}_I = \boldsymbol{R}_0 + \boldsymbol{R}\boldsymbol{Z}_D + \boldsymbol{\varepsilon}_R, \tag{S.5}$$

where $\boldsymbol{R}$ represents the correlation matrix between $\boldsymbol{Z}_I$ and Z_D, $\boldsymbol{R}_0$ is independent with $\boldsymbol{Z}_D$, and $\boldsymbol{\varepsilon}_R$ is independent with $\boldsymbol{Z}_D$. On the other hand, $\boldsymbol{Z}_E$ is independent with $\boldsymbol{Z}_D$, then we can rewrite equation (6) as

$$
\begin{aligned}
Y &= \gamma_0 + \boldsymbol{\gamma}_D^T \boldsymbol{Z}_D + \boldsymbol{\gamma}_I^T \boldsymbol{Z}_I + \boldsymbol{\gamma}_E^T \boldsymbol{Z}_E + \varepsilon_Y \\
&= (\beta\boldsymbol{\alpha} + \boldsymbol{\eta})^T \boldsymbol{Z}_D + \boldsymbol{\gamma}_I^T (\boldsymbol{R}_0 + \boldsymbol{R}^T \boldsymbol{Z}_D + \boldsymbol{\varepsilon}_R) + \boldsymbol{\gamma}_E^T \boldsymbol{Z}_E + \varepsilon_Y \\
&= \beta\boldsymbol{\alpha}^T \boldsymbol{Z}_D + (\boldsymbol{\eta} + \boldsymbol{R}\boldsymbol{\gamma}_I)^T \boldsymbol{Z}_D + (\boldsymbol{\gamma}_R^T \boldsymbol{R}_0 + \boldsymbol{\gamma}_E^T \boldsymbol{Z}_E) + \boldsymbol{\gamma}_I^T \boldsymbol{\varepsilon}_R + \varepsilon_Y \\
&= \beta X + (\boldsymbol{\eta} + \boldsymbol{R}\boldsymbol{\gamma}_I)^T \boldsymbol{Z}_D + (\boldsymbol{\gamma}_R^T \boldsymbol{R}_0 + \boldsymbol{\gamma}_E^T \boldsymbol{Z}_E - \beta\alpha_0) + (\boldsymbol{\gamma}_I^T \boldsymbol{\varepsilon}_R \\
&\quad + \varepsilon_Y - \beta\varepsilon_X) \\
&= \beta_0 + \beta X + \tilde{\boldsymbol{\gamma}}^T \boldsymbol{Z}_D + \tilde{\varepsilon}_Y,
\end{aligned} \tag{S.6}
$$

where $\beta_0 = \boldsymbol{\gamma}_R^T \boldsymbol{R}_0 + \boldsymbol{\gamma}_E^T \boldsymbol{Z}_E - \beta\alpha_0$, $\tilde{\boldsymbol{\gamma}} = \boldsymbol{\eta} + \boldsymbol{R}\boldsymbol{\gamma}_I$, and $\tilde{\varepsilon}_Y = \boldsymbol{\gamma}_I^T \boldsymbol{\varepsilon}_R + \varepsilon_Y - \beta\varepsilon_X$. $\tilde{\varepsilon}_Y$ is independent with $\boldsymbol{Z}_D$. Then we have

$$
\begin{aligned}
X &= \alpha_0 + \boldsymbol{\alpha}^T \boldsymbol{Z}_D + \varepsilon_X, \\
Y &= \beta_0 + \beta X + \tilde{\boldsymbol{\gamma}}^T \boldsymbol{Z}_D + \tilde{\varepsilon}_Y,
\end{aligned} \tag{S.7}
$$

where ε_X and $\tilde{\varepsilon}_Y$ are correlated, but both independent with $\boldsymbol{Z}_D$. The total error term ε_X and $\tilde{\varepsilon}_Y$ can be decomposed into a confounding-related term and a completely random term, then we have $\mathbb{E}(\varepsilon_X) = \mathbb{E}(\tilde{\varepsilon}_Y) = 0$, $\mathrm{Var}(\varepsilon_X) = \delta_1^2 + \sigma_1^2$, and $\mathrm{Var}(\tilde{\varepsilon}_Y) = \delta_2^2 + \sigma_2^2$.

It is not necessary to identify all variants in $\mathcal{Z}_D$. We only need to select a subset of $\mathcal{Z}_D$ as instruments. In other words, it is essential to identify $\mathcal{Z}_D$ via BN learning with a high specificity instead of sensitivity. If we select genetic $Z_j \in \mathcal{Z}_D$ $(j = 1, 2, \ldots, J)$ as instruments, we have the Bayesian MR model [5]

$$
\begin{aligned}
X | Z, U &\sim \mathcal{N}(\alpha_0 + \sum_{j=1}^{J} \alpha_j Z_j + \delta_1 U, \sigma_1^2) \\
Y | X, Z, U &\sim \mathcal{N}(\beta_0 + \beta X + \sum_{j=1}^{J} \gamma_j Z_j + \delta_2 U, \sigma_2^2), \\
U &\sim \mathcal{N}(0, 1).
\end{aligned}
\tag{S.8}
$$

The explicit modeling of pleiotropic effects brings nuisance parameters. To make the causal effect of interest β identifiable, we make an assumption that not all instruments included in the model have non-zero pleiotropic effect. And therefore, we impose a shrinkage prior on $\boldsymbol{\gamma}$ under the Bayesian framework [5]. Each component of $\boldsymbol{\alpha}$ has an independent Gaussian prior, and uninformative uniform priors are used for the other parameters.

Therefore, the BNMR model can be used to estimate the causal effect between exposure and outcome in two steps. In the learning stage, $\mathcal{Z}_D$ is distinguished from $\mathcal{Z}_I$ and $\mathcal{Z}_E$ through BN structure learning with all the variants and exposure X. In the inference stage, using selected Z_j as IVs, the causal effects can be estimated via the above Bayesian MR equation (S.8).

For non-Gaussian distributed outcomes, we introduce the link function $h(\cdot)$ for transformation, i.e.

$$
h(\mathbb{E}(Y | X, Z, U)) = \beta_0 + \beta X + \sum_{j=1}^{J} \gamma_j Z_j + \delta_2 U.
\tag{S.9}
$$

For example, we can use logistic regression for binary outcome, and here the link function $h(y) = \mathrm{logit}(y) = \log \frac{y}{1-y}$.

SN2 Adjacency score and relevance strength

When all variants are included in each subsample ($p_s = p$), the adjacency score of a particular variant Z_i can be regarded as the confidence of the edge $Z_i - X$ in the average graph, or the probability that Z_i belongs to subset $\mathcal{Z}_D$. When $p_s < p$, the adjacency score can be regarded as the "relative probability" that Z_i belongs to subset $\mathcal{Z}_D$ since all variants share the same likelihood to be sampled in each subgraph. Variants with higher adjacency score are more reliable to affect
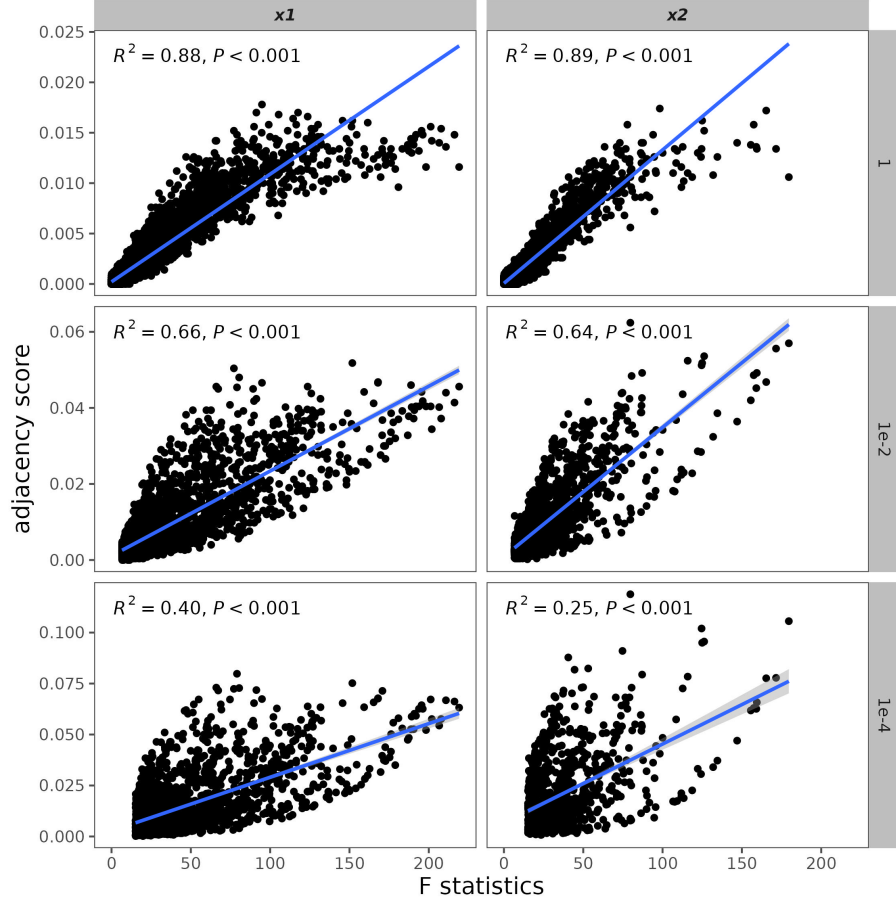
Figure S2: Correlation between F statistics and adjacency scores. The rows represent the P threshold before BN learning, and the columns represent the exposure of interest.

the exposure of interest, and therefore, it is also an assessment of relevance strength.

We explore the correlation between adjacency scores obtained via RGF and F statistics, a widely-used indicator of instrument strength, using the larger simulated dataset (n = 10000, p = 10000). The hyperparameters of RGF are set as n_s = 5000, p_s = 150, r = 1000. Strong positive correlation exists when no primary screening is performed prior to the BN structure learning. With smaller P threshold are used, fewer variants are examined in the RGF, and the correlation strength becomes weaker (Figure S2).

SN3 Performance of BN in the presence of epistasis

We simulate phenotypes from the combination of three polygenetic models including simple multiplicative effects, interactive multiplicative effects, and interactive threshold effects (Table S1) [6], so as to appraise the performance of BN in settling the puzzle of gene interaction and epistasis.

- Simple Multiplicative Model: Each locus individually affects the phenotype with cumulative effects within and between loci. Each additional risk allele increases the effect with a multiplier (θ_1 for allele A and θ_2 for allele B).

- Interactive Multiplicative Model: Both loci interactively affect the phenotype with cumulative effects. Each additional risk allele increases the effect with a multiplier θ only when the risk allele in both loci are present together.

- Interactive Threshold Model: The presence of risk alleles in both loci increases the effect with a multiplier θ without cumulative effects.

Table S1: Polygenetic model

model 1	aa	Aa	AA
bb	α	$\alpha(1+\theta_1)$	$\alpha(1+\theta_1)^2$
Bb	$\alpha(1+\theta_2)$	$\alpha(1+\theta_1)(1+\theta_2)$	$\alpha(1+\theta_1)^2(1+\theta_2)$
BB	$\alpha(1+\theta_2)^2$	$\alpha(1+\theta_1)(1+\theta_2)^2$	$\alpha(1+\theta_1)^2(1+\theta_2)^2$
model 2	aa	Aa	AA
bb	α	α	α
Bb	α	$\alpha(1+\theta)$	$\alpha(1+\theta)^2$
BB	α	$\alpha(1+\theta)^2$	$\alpha(1+\theta)^4$
model 3	aa	Aa	AA
bb	α	α	α
Bb	α	$\alpha(1+\theta)$	$\alpha(1+\theta)$
BB	α	$\alpha(1+\theta)$	$\alpha(1+\theta)$

The complex gene interaction pattern is simulated as combinations of a series of simple patterns (Figure S3). In each simple pattern, phenotype X_1 is determined by loci G_A and G_B through one of the above three polygenetic models, while phenotype X_2 is determined by loci G_A and G_M. Loci G_S is in LD with G_A (S-A) and loci G_T is in reverse LD with G_B (T-b). We set $\pi_A = 0.15$, $\pi_B = 0.20$, $\pi_M = 0.16$, $\pi_S = 0.25$, $\pi_T = 0.3$, $r_A S = 0.7$, $r_B T = -0.6$, $\alpha = 0.2$ for X_1 and $\alpha' = 0.15$ for X_2 in each simple pattern. In simple
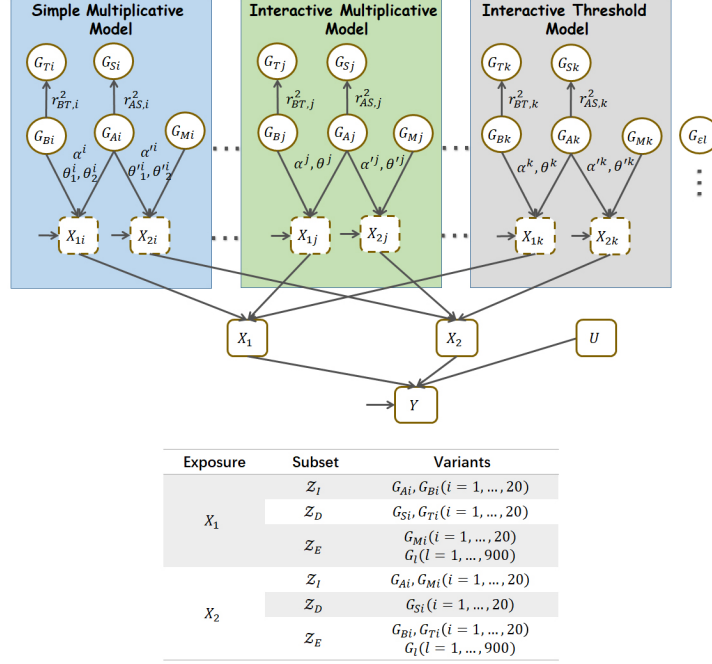
Figure S3: The polygenetic model.

multiplicative model, we set $\theta_1 = 0.3$, $\theta_2 = 0.5$ for X_1 and $\theta'_1 = 0.4$, $\theta'_2 = 0.4$ for X_2. In interactive multiplicative model and interactive threshold model, we set $\theta = 0.3$ for X_1 and $\theta' = 0.5$ for X_2. The environmental variance of X_1 is larger to represent traits with lower heritability. The complex pattern is a combination of 60 simple patterns, in which every 20 simple patterns follow a kind of polygenetic model. The ultimate phenotypes X_1 and X_2 is the average of corresponding phenotypes in each simple pattern. We generated other 900 uncorrelated variants. 5000 subjects are sampled in total.

We use the RGF with $n_s = 5000$, $p_s = 150$, $r = 1000$ to select variants belonging to $\mathcal{Z}_D$. The results (Figure S4) reveal that RGF can identify true effect variants with remarkably low false discovery rate (FDR) in the presence of complex gene interaction and epistasis, especially for traits with higher heritability.
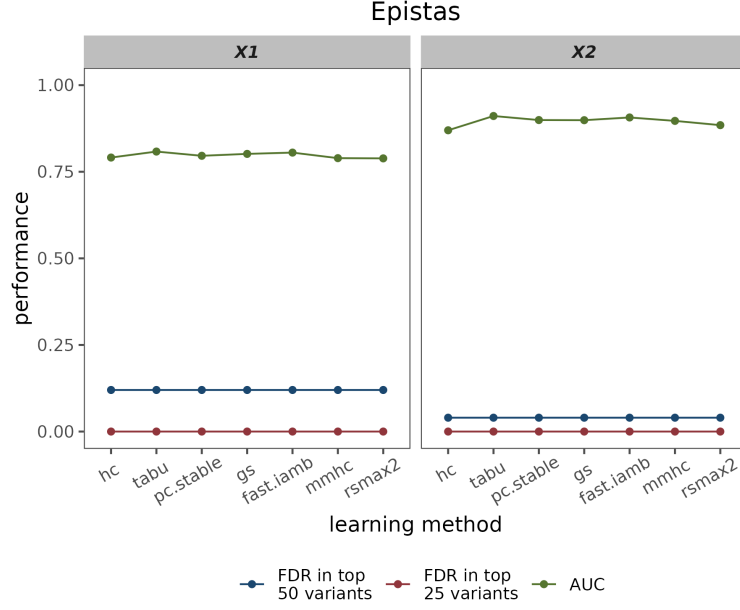
Figure S4: The performance of RGF in the presence of epistasis.

SN4 Sensitivity analysis on IV numbers and iterations

The numbers of iterations and instruments are hyperparameters that need to be specified artificially in advance in BNMR model. For example, one can specify top n^* variants in adjacency scores or variants with adjacency score larger than $\frac{\alpha^* p_s}{p}$ as instruments, where α^* is a given threshold between 0 and 1. Previous researches and experience may benefit the choice but lacks theoretical criteria and explanations. Here we conduct sensitivity analysis using Bayesian MR with different numbers of instruments and iterations in simulations. Instruments are selected according to the ranks of RGF adjacency scores. We want to demonstrate how the changes in hyperparameters affect the properties of estimation (bias, variance, and convergence) as well as time consumption, and examine the stability of BNMR model for different settings.

The sensitivity analysis (Tables S2 & S3, Figures 5 a & b) confirm that robust estimates can be obtained via BNMR. The time consumption increases when the numbers of instruments and iterations increase. Bias increases when there are too many or too few instruments. Good convergence when 5000 iterations have been made according to the Rhat.

Table S2: Sensitivity analysis on different IV number [1]

IV number	time/min	bias	SE	Rhat
10	73.80	2.07	0.064	1.11
20	84.26	2.01	0.031	1.03
40	96.91	2.01	0.027	1.02
60	126.83	2.01	0.025	1.05
100	249.27	2.00	0.025	1.04
150	393.66	2.02	0.024	1.04

[1] The estimation is conducted using simulated data of scenario "50+50" in Table 2. Four chains and 5000 iterations per chain are used under horseshoe prior.

Table S3: Sensitivity analysis on different iterations [1]

IV number	time/min	bias	SE	Rhat
1000	15.01	2.00	0.024	1.22
2000	34.42	2.01	0.029	1.10
5000	64.94	2.00	0.030	1.02
10000	143.69	2.00	0.030	1.01
20000	227.97	2.00	0.029	1.01

[1] 20 instruments are used under horseshoe prior. 60% of them have pleiotropic effects. Four chains are used for sampling.

SN5 Performance of different shrinkage priors

Bayesian estimation with imposed shrinkage priors is conceptually similar to regularization in the traditional model but with some obvious advantages. The penalty parameters can be estimated simultaneously with the model parameters and standard errors of parameters can be obtained directly from posterior distributions. Bayesian models are also more intuitive to establish and interpret, and specific expert knowledge can be included into the model as informative priors. Additionally, Bayesian sampling of posterior distributions though Markov Chain Monte Carlo (MCMC) can avoid the difficulties of traditional regularization methods in solving optimization problems.

We demonstrate the performance of different shrinkage priors in Bayesian MR estimation using RStan [7]. Here we discuss the following commonly used priors [8].

- Bayesian Lasso

$$\gamma_j | \lambda \sim Double - Exp(0, \frac{1}{\lambda})$$
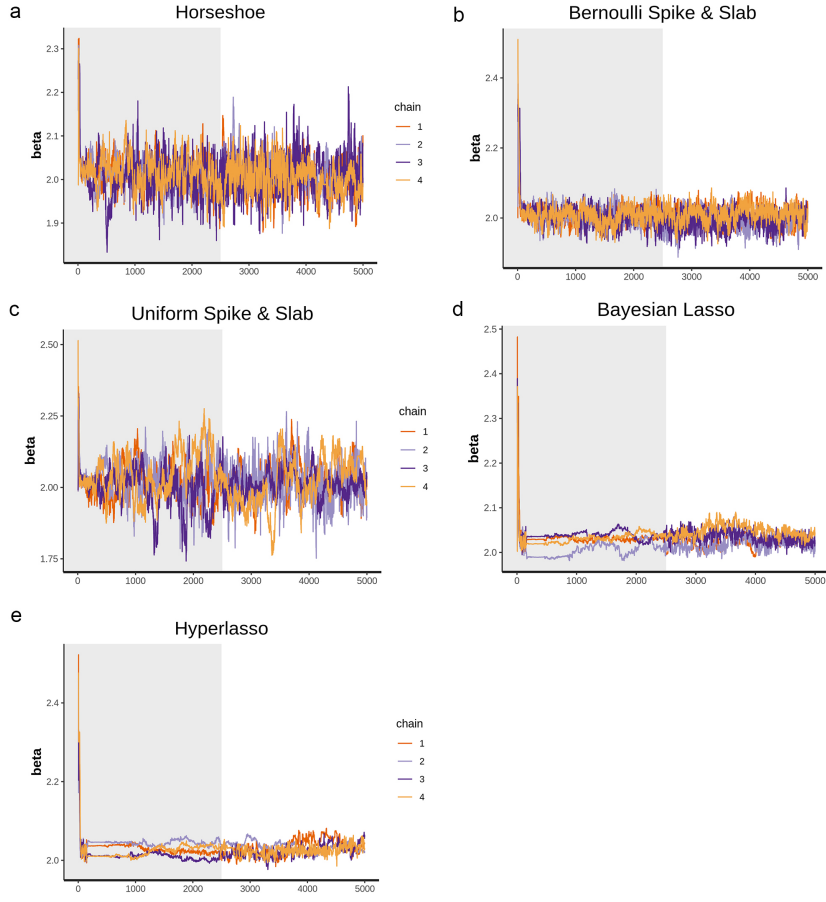$$\lambda \sim Cauchy^+(0, 1)$$

(S.10)

Figure S5: The trace plots of MCMC with different shrinkage priors.

- Hyperlasso

$$
\begin{aligned}
\gamma_j | \tau_j &\sim Double - Exp(0, \sqrt{2\tau_j}) \\
\tau_j | \lambda &\sim \Gamma(0.5, \frac{1}{\lambda^2}) \\
\lambda &\sim Cauchy^+(0, 1)
\end{aligned}
\tag{S.11}
$$

- Uniform spike & slab

$$
\begin{aligned}
\gamma_j | \lambda_j, \tau_j &\sim \lambda_j \mathcal{N}(0, \tau_j) \\
\tau_j &\sim IG(0.5, 0.5) \\
\lambda &\sim U(0, 1)
\end{aligned}
\tag{S.12}
$$

- Bernoulli spike & slab

$$\gamma_j | \lambda_j, \tau_j \sim \lambda_j \mathcal{N}(0, \tau_j) + (1 - \lambda_j) \mathcal{N}(0, 0.001)$$
$$\tau_j \sim IG(0.5, 0.5)$$
$$\lambda_j | \pi \sim Bernoulli(\pi) \tag{S.13}$$
$$\pi \sim U(0, 1)$$

- Horseshoe

$$\gamma_j | \phi_j \sim N(0, \phi_j)$$
$$\phi_j | \tau \sim Cauchy^+(0, \tau) \tag{S.14}$$
$$\tau \sim Cauchy^+(0, 1)$$

Here we use $Cauchy^+(\mu, \sigma)$ to represent half-Cauchy distribution with location parameter μ and scale parameter σ, $IG(\alpha, \beta)$ to represent inverse-Gamma distribution with location parameter α and scale parameter β, $Double-Exp(\mu, \sigma)$ to represent double-exponential (Laplace) distribution with location parameter μ and scale parameter σ, $\Gamma(\alpha, \beta)$ to represent Gamma distribution with location parameter α and rate parameter β.

Table S4: The performance of different shrinkage priors [1]

prior	time/min	bias	SE	Rhat
horseshoe	57.00	0.007	0.036	1.05
uniform spike & slab	73.96	0.023	0.060	1.11
Bernoulli spike & slab	34.74	0.002	0.025	1.13
lasso	7.90	0.031	0.015	1.36
hyperlasso	45.74	0.034	0.015	1.34

[1] For chains with 5000 iterations per chain and 20 instruments are used.

We use 20 instruments in MR estimations, 60% of which have a pleiotropic effect. There are 5000 iterations in MCMC with 4 chains, and the first half is used as burn-in. The results (Table S4, Figures 5c & S5) show that all these priors can obtain a relatively unbiased estimation. The Bayesian Lasso prior has the fastest sampling speed, while the horseshoe prior is superior in convergence.

SN6   Instruments used in application

Variants with top 50 adjacency scores are selected as instruments in application. The variants rsID are reported according to Genome Reference Consortium Human Build 37 patch release 13 (GRCh37.p13) (`https://www.ncbi.nlm.nih.gov/assembly/GCF_000001405.25`).

Instruments of RBC

Strict GWAS P threshold (1e-20) in pre-filtering + BNMR:
rs9376090, rs4895440, rs34164109, rs7775698, rs7776054, rs9402685, rs6920211, rs9402686, rs7758845, rs35786788, rs11759553, rs9494142, rs9389269, rs35959442, rs56293029, rs9376091, rs9399137, rs9494145, rs9389268, rs9373124;
Loose GWAS P threshold (5e-8) in pre-filtering with LD clumping (threshold: window = 10000kb, r^2=0.01, MAF=0.01) + BNMR:
rs9399136, rs218265, rs221788, rs9349205, rs10495928, rs9487023, rs550057, rs56397034, rs10224210, rs41294850, rs78744187, rs17476364, rs7137828, rs592423, rs6592965, rs10758656, rs55938136, rs3809627, rs10849020, rs79301522.

Instruments of HGB

Strict GWAS P threshold (1e-20) in pre-filtering + BNMR:
rs72805692, rs17476364, rs79220007, rs1800562, rs16926246, rs79920061, rs16926249, rs113041162, rs55925606, rs73265749, rs144861591, rs1408272, rs80215559, rs115740542, rs10159477, rs10168349, rs198851, rs116009877, rs2032451, rs129128;
Loose GWAS P threshold (5e-8) in pre-filtering with LD clumping (threshold: window = 10000kb, r^2=0.01, MAF=0.01) + BNMR:
rs17476364, rs144861591, rs1799945, rs10495928, rs7137828, rs635634, rs73158188, rs9402685, rs10901252, rs61739556, rs13107325, rs6665764, rs55893317, rs12819124, rs7778978, rs174533, rs115986297, rs11072567, rs8887, rs123698.

Instruments of HCT

Strict GWAS P threshold (1e-20) in pre-filtering + BNMR:
rs17476364, rs72805692, rs16926246, rs16926249, rs73265749, rs113041162, rs10159477, rs7775698, rs4953318, rs9376090, rs10495928, rs9373124, rs34164109, rs9402685, rs1331309, rs9389269, rs653178, rs9399136, rs9376091, rs9402686;
Loose GWAS P threshold (5e-8) in pre-filtering with LD clumping (threshold: window = 10000kb, r^2=0.01, MAF=0.01) + BNMR:
rs17476364, rs9402685, rs10495928, rs6464165, rs7137828, rs144861591, rs635634, rs1799945, rs221788, rs61739556, rs55893317, rs4282786, rs2732480, rs218265, rs115986297, rs123698, rs13107325, rs4886755, rs2029466, rs55938136.

Instruments of MCV

Strict GWAS P threshold (1e-20) in pre-filtering + BNMR:
rs4895441, rs1800562, rs635243, rs34164109, rs628751, rs55925606, rs66717417, rs112233623, rs9471709, rs9402685, rs589235, rs1799945, rs9373124, rs6920211, rs634869, rs116009877, rs11970772, rs56293029, rs592423, rs1408272;
Loose GWAS P threshold (5e-8) in pre-filtering with LD clumping (threshold: window = 10000kb, r^2=0.01, MAF=0.01) + BNMR:
rs9399136, rs9471708, rs144861591, rs592423, rs198851, rs218265, rs9487023, rs7853365, rs6014993, rs9381093, rs9866958, rs2238368, rs7385804, rs6592965, rs9816784, rs8887, rs56397034, rs41294850, rs4890633, rs62160676.

Instruments of lymphocyte count

rs3184504, rs10422126, rs9494142, rs79237520, rs7939778, rs79478560, rs11746, rs72781680, rs56987668, rs8064314, rs6568490, rs6806966, rs4544902, rs2157691, rs2229092, rs78398999, rs6832951, rs13315469, rs2326837, rs7689637;

Instruments of SCZ

rs111484181, rs118065847, rs146125378, rs72672191, rs145192171, rs185264641, rs142746289, rs77387634, rs117533018, rs7817793, rs114490061, rs75313396, rs548779843, rs7193015, rs9655954, rs56329281, rs75138255, rs112215928, rs72719202, rs72842009, rs79245731.

SN7   Comparison with conventional methods in application

We conduct the MR analysis using existing MR procedures. In Table S5, we report estimates from our BNMR method and other three existing approaches (TSLS, penalized robust MR-Egger, and CIIV). The conpared methods use lead SNPs after LD clumping by R package ieugwasr as instruments. TSLS is implemented with R package AER, penalized robust MR-Egger estimator is implemented with R package MendelianRandomization [9], and CIIV is implemented with R package CIIV. We can find that estimates vary significantly when using different IVs and MR approaches.

The results indicate that appropriate instruments and estimation methods are vital in MR analysis. The results of MR should be taken with caution, and need more triangulating evidence from other non-MR designs [10].

SN8   Gene mapping and functional annotation for SCZ and lymphocyte

In addition to instrument selection, our simulations suggest RGF is also a useful fine-mapping tool to prioritize effect variants in post-GWAS analysis. Using FUMA [11], we conduct gene mapping and functional annotation for top 1500 variants identified through RGF for SCZ and lymphocyte count, respectively. FUMA maps 303 lymphocyte-related protein-coding genes and 36 SCZ-related protein-coding genes.

We explore the tissue-differentially expressed genes (DEG) and conduct enrichment analysis. Figure S6 & S7 show the expression heatmap and MAGMA tissue expression differences of 36 mapped SCZ-related genes. Figure S8 shows the expression heatmap of 303 mapped lymphocyte-related genes.

Table S5: Results of different MR approaches in real data application

exposure	outcome	TSLS			penalized robust MR-Egger			CIIV				BNMR			
		beta	se	P	beta	se	P	beta	se	2.5% CI	97.5% CI	beta	se	2.5% CI	97.5% CI
RBC	DBP	2.239	0.293	0.000	0.444	2.748	0.872	1.426	0.322	0.796	2.057	6.935	0.076	6.472	7.431
RBC	SBP	0.632	0.544	0.246	-0.355	2.759	0.898	-0.359	0.518	-1.374	0.656	8.946	0.067	7.312	10.097
HGB	DBP	1.417	0.131	0.000	1.575	1.309	0.229	1.541	0.187	1.174	1.909	2.226	0.237	1.815	2.608
HGB	SBP	0.446	0.246	0.070	1.872	1.405	0.183	-0.577	0.279	-1.125	-0.030	3.362	0.316	2.738	3.897
HCT	DBP	0.475	0.046	0.000	0.558	0.504	0.268	0.569	0.063	0.446	0.692	0.745	0.256	0.593	0.851
HCT	SBP	0.083	0.087	0.337	0.651	0.529	0.218	-0.219	0.095	-0.404	-0.033	1.093	0.862	0.957	1.214
MCV	DBP	0.031	0.018	0.096	0.154	0.118	0.191	-0.081	0.022	-0.125	-0.038	-0.084	0.065	-0.193	0.038
MCV	SBP	0.025	0.034	0.460	0.076	0.126	0.545	-0.019	0.035	-0.088	0.049	-0.020	0.066	-0.158	0.106
lymphocyte	SCZ				4.722	1.879	0.012					0.234	0.102	0.038	0.435
lymphocyte	PTSD				1.649	1.702	0.332					0.222	0.347	-0.322	1.040
SCZ	lymphocyte				-0.144	0.425	0.734					0.117	0.119	-0.094	0.373

Figure S6: Expression heatmap of SCZ-related genes in GTEx v8 30 general tissue types (a) and GTEx v8 53 tissue types (b).
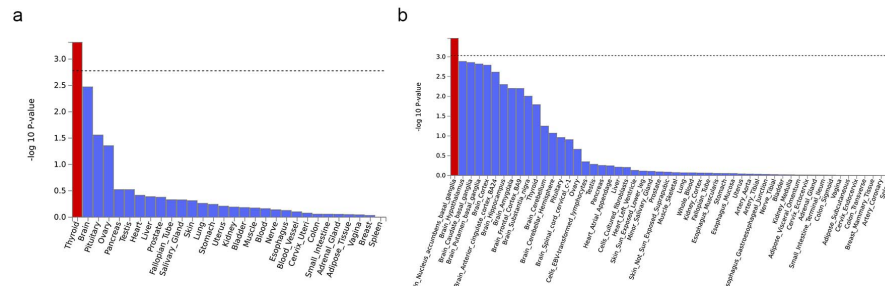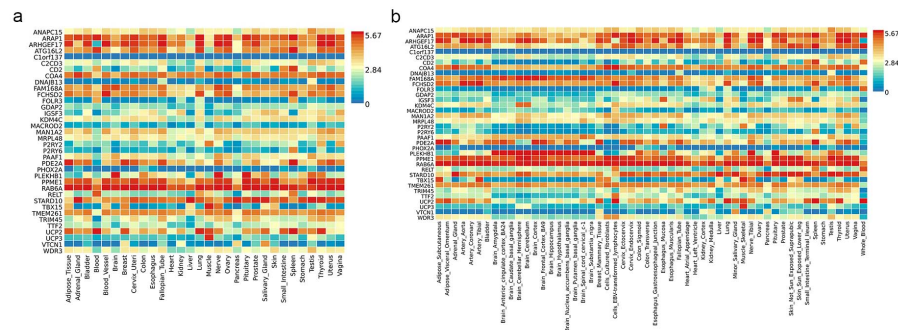

Figure S7: MAGMA tissue expression analysis for mapped SCZ-related genes in GTEx v8 30 general tissue types (a) and GTEx v8 53 tissue types (b).

References

[1] Richard Howey, So-Youn Shin, Caroline Relton, George Davey Smith, and Heather J Cordell. Bayesian network analysis incorporating genetic anchors complements conventional Mendelian randomization approaches for exploratory analysis of causal relationships in complex data. *PLoS Genetics*, 16(3):e1008198, 2020.

[2] Ana Rita Nogueira, Andrea Pugnana, Salvatore Ruggieri, Dino Pedreschi, and João Gama. Methods and tools for causal discovery and causal inference. *Wiley Interdisciplinary Reviews: Data Mining and Knowledge Discovery*, 12(2):e1449, 2022.

[3] Marco Scutari. Learning Bayesian networks with the bnlearn R package. *Journal of Statistical Software*, 35(3):1–22, 2010.
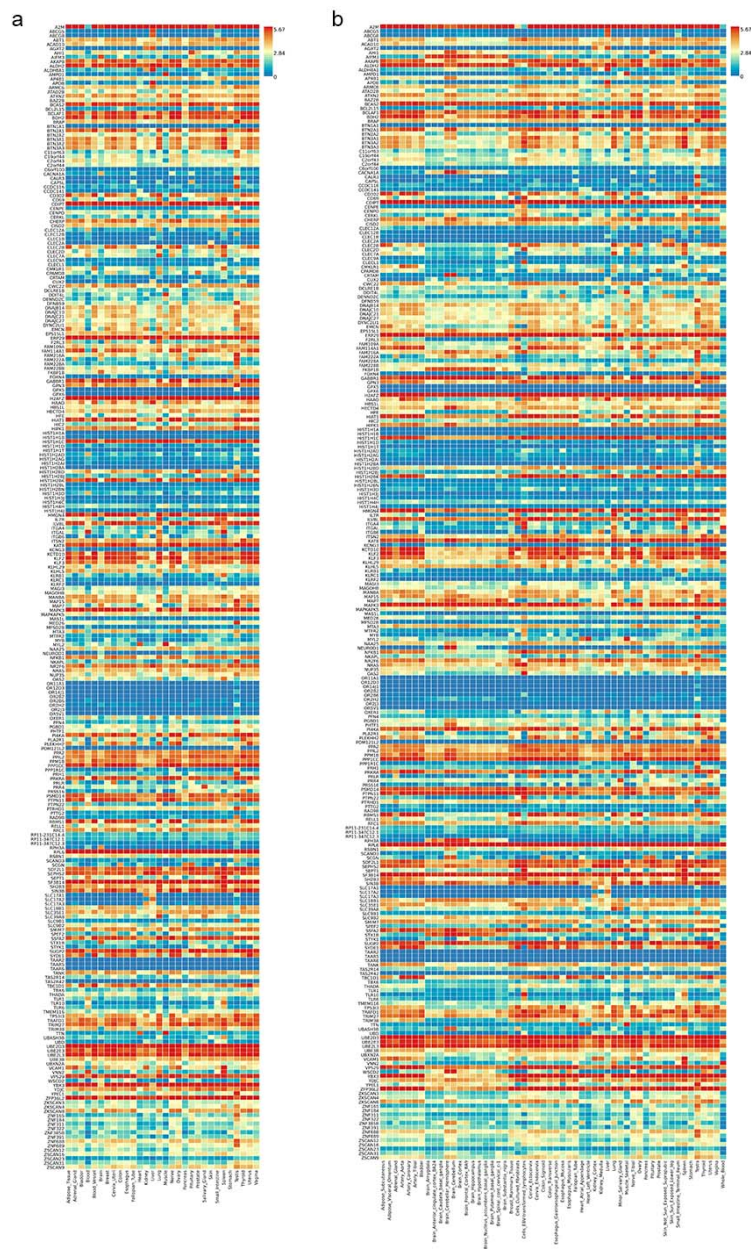
Figure S8: Expression heatmap of lymphocyte-related genes in GTEx v8 30 general tissue types (a) and GTEx v8 53 tissue types (b).

[4] Jean-Baptiste Pingault, Paul F O'reilly, Tabea Schoeler, George B Ploubidis, Frühling Rijsdijk, and Frank Dudbridge. Using genetic data to strengthen causal inference in observational research. *Nature Reviews Genetics*, 19(9):566–580, 2018.

[5] Carlo Berzuini, Hui Guo, Stephen Burgess, and Luisa Bernardinelli. A Bayesian approach to Mendelian randomization with multiple pleiotropic variants. *Biostatistics*, 21(1):86–101, 2020.

[6] Jonathan Marchini, Peter Donnelly, and Lon R Cardon. Genome-wide strategies for detecting multiple loci that influence complex diseases. *Nature Genetics*, 37(4):413–417, 2005.

[7] Bob Carpenter, Andrew Gelman, Matthew D Hoffman, Daniel Lee, Ben Goodrich, Michael Betancourt, Marcus Brubaker, Jiqiang Guo, Peter Li, and Allen Riddell. Stan: A probabilistic programming language. *Journal of Statistical Software*, 76(1), 2017.

[8] Sara Van Erp, Daniel L Oberski, and Joris Mulder. Shrinkage priors for Bayesian penalized regression. *Journal of Mathematical Psychology*, 89:31–50, 2019.

[9] Olena O Yavorska and Stephen Burgess. Mendelianrandomization: an R package for performing Mendelian randomization analyses using summarized data. *International Journal of Epidemiology*, 46(6):1734–1739, 2017.

[10] Debbie A Lawlor, Kate Tilling, and George Davey Smith. Triangulation in aetiological epidemiology. *International Journal of Epidemiology*, 45(6):1866–1886, 2016.

[11] Kyoko Watanabe, Erdogan Taskesen, Arjen Van Bochoven, and Danielle Posthuma. Functional mapping and annotation of genetic associations with FUMA. *Nature Communications*, 8(1):1826, 2017.